Aquat Geochem (2012) 18:45–75
DOI 10.1007/s10498-011-9148-x

ORIGINAL PAPER

Water–Rock Interactions: An Investigation of the Relationships Between Mineralogy and Groundwater Composition and Flow in a Subtropical Basalt Aquifer

Katrina L. Locsey · Micaela Grigorescu · Malcolm E. Cox

Received: 23 May 2009 / Accepted: 26 September 2011 / Published online: 12 October 2011

Abstract A holistic study of the composition of the basalt groundwaters of the Atherton Tablelands region in Queensland, Australia was undertaken to elucidate possible mechanisms for the evolution of these very low salinity, silica- and bicarbonate-rich groundwaters. It is proposed that aluminosilicate mineral weathering is the major contributing process to the overall composition of the basalt groundwaters. The groundwaters approach equilibrium with respect to the primary minerals with increasing pH and are mostly in equilibrium with the major secondary minerals (kaolinite and smectite), and other secondary phases such as goethite, hematite, and gibbsite, which are common accessory minerals in the Atherton basalts. The mineralogy of the basalt rocks, which has been examined using X-ray diffraction and whole rock geochemistry methods, supports the proposed model for the hydrogeochemical evolution of these groundwaters: precipitation + CO_2 (atmospheric + soil) + pyroxene + feldspars + olivine yields H_4SiO_4, HCO_3^-, Mg^{2+}, Na^+, Ca^{2+} + kaolinite and smectite clays + amorphous or crystalline silica + accessory minerals (hematite, goethite, gibbsite, carbonates, zeolites, and pyrite). The variations in the mineralogical content of these basalts also provide insights into the controls on groundwater storage and movement in this aquifer system. The fresh and weathered vesicular basalts are considered to be important in terms of zones of groundwater occurrence, while the fractures in the massive basalt are important pathways for groundwater movement.

Keywords Basalt aquifer · Aluminosilicate mineral weathering · Mass balance

1 Introduction

The composition of groundwater may be regarded as a function of the sources and sinks of the chemical elements along the groundwater flow path (Deutsch 1997). In a chemical

K. L. Locsey · M. Grigorescu (✉) · M. E. Cox
School of Natural Resource Sciences, Queensland University of Technology, Brisbane, QLD, Australia
e-mail: m.preda@qut.edu.au
URL: www.qut.edu.au

weathering study of a watershed in the south-eastern United States, for example, Cleaves et al. (1974) noted that the construction of a weathering model and a geochemical balance requires integration of water chemistry and mineralogical data. Benedetti et al. (1999) observed that few studies integrate water chemistry and mineralogical data and recommend that interpretations of likely water–rock interactions should not be based on solutions equilibria calculations alone, but taken in conjunction with known mineralogical associations.

A holistic approach has been applied to a chemical weathering study of the basalt aquifer system of the Atherton Tablelands, North Queensland, Australia.

The mineralogy of three basalt profiles has been examined in detail, based on X-ray diffraction (XRD) analyses and major element geochemistry of drill chip samples collected during a groundwater bore drilling program. The chemical characteristics of the Atherton Tablelands groundwaters have been interpreted in terms of the mineralogical composition of the basalt, weathered zone, interbeds, and basement rocks. In addition, the mineralogy and water chemistry of the tropical Atherton groundwater system has been compared to other basalt aquifers worldwide. The influences of other hydrogeochemical processes on the groundwater composition were also investigated and a mass balance for the aquifer calculated. The methodology employed in this study has enabled the formulation of a hypothesis for the hydrogeochemical evolution of the basalt groundwater.

2 Setting

The Atherton Tablelands is located approximately 70 km south-west of Cairns, a regional city in North Queensland, Australia (Fig. 1). This plateau has a subtropical monsoonal climate, with a mean annual temperature of around 24°C and rainfall decreasing from the south-east (approximately 2,700 mm at Millaa Millaa) to the north-west (approximately 1,300 mm at Tolga). The Atherton Tablelands is characterized by deep soil and weathered basalt profiles, a result of the high rainfall and temperatures in the region. Two major catchments drain the study area, with the Barron River flowing to the north and the North Johnstone River flowing to the south. The Barron River and Mazlin Creek flow into Lake Tinaroo, a water supply reservoir.

Most of the arable land of the plateau has been cleared for agriculture and dairying, with widespread irrigation in the north-eastern part of the Tablelands. Demand for groundwater has resulted in declining water levels over the last 20 years, particularly in the northern parts of the study area.

3 Geology

The study area is located within the basaltic lava field of the Atherton Basalt Province (ABP), which forms part of the Eastern Australia Volcanic Zone (EAVZ) (Stephenson 1989). The EAVZ is a zone of intraplate volcanism extending discontinuously along the entire east coast of Australia, which was formed by plumes of mantle material that travelled through the Indian plate (Wellman and McDougall 1974; Sutherland 1983). The ABP covers an area of approximately 1,800 km^2 and contains 52 reported volcanic centers (Stephenson et al. 1980). These volcanic features include shield volcanoes, composite cones, maars, cinder cones, and one diatreme (Stephenson et al. 1980). The basaltic rocks

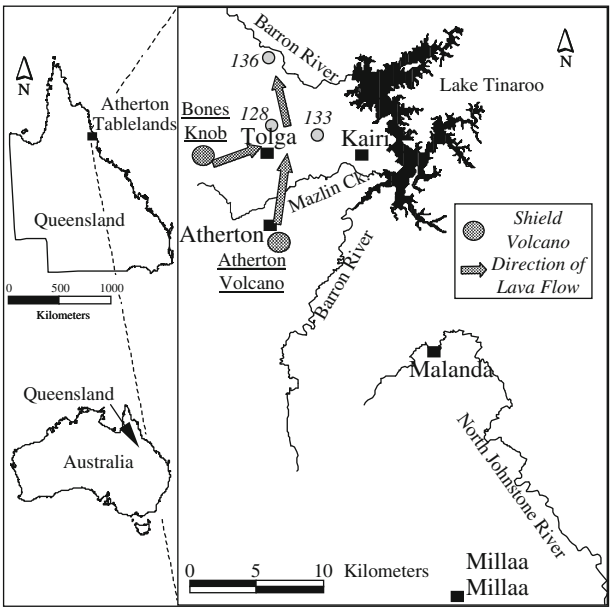

Fig. 1 Location of the Atherton Tablelands in North Queensland, including major shield volcanoes in the northern part of the study area, inferred directions of lava flow, and the locations of groundwater bores 11000128, 11000133, and 11000136 from which mineralogical profiles have been constructed

within the study area are currently dated to a maximum of 3.1 Ma (Stephenson et al. 1980), with the volcanic features east of Tolga dated at 1.7–1.8 Ma (Stephenson 1989).

The basaltic rocks in the study area range from extremely massive to highly vesicular and are fresh to highly weathered. Phenocrysts of olivine, augite, and rarely plagioclase are present in the majority of flows; occasional samples are aphyric. Highly weathered, clay-rich palaeosols are common between basalt flows. The basaltic rocks in the ABP (not including pyroclastic material) have been classified into four groups based on the CIPW normative mineralogies of 35 samples: olivine tholeiites, alkali olivine basalts, basanites, and one quartz tholeiite. The most abundant rocks in the ABP are the olivine tholeiites and alkali olivine basalts (Sheldrick 1999). The following descriptions are from Sheldrick (1999):

> The olivine tholeiites contain phenocrysts of olivine (composition Fo77-85, with rims typically Fo58-62), and pyroxenes ranging from augite to endiopside. The groundmass comprises a fine-grained mixture of pyroxenes (mostly augite), olivine (Fo48-60) and plagioclase feldspars ranging from oligoclase to labradorite (An20-62). The alkali olivine basalts also contain olivine phenocrysts (Fo74-85) with more iron-rich rims (Fo64-71), as well as the pyroxenes diopside, endiopside and salite. The groundmass similarly comprises plagioclase feldspars, with a composition ranging from oligoclase to labradorite (An28-70), as well as the pyroxenes augite, salite and rare pigeonite (with a lesser Ca content). The basanites contain olivine phenocrysts (Fo85-90) set in a groundmass of clinopyroxene. Accessory minerals in the basaltic rocks include ilmenite, titano-magnetite and apatite.

4 Hydrogeology

The basalt aquifer system of the Atherton Tablelands comprises a sequence of basaltic rocks commonly 50–100 m thick, with a weathered profile of up to 30 m. Standing water levels in the region are generally 15–40 m below the ground surface, and seasonal variations in water levels can be up to 20 m. The groundwater flow directions generally follow the surface topography and, in the north-eastern part of the study area, flow directions are mostly toward the north–north-west. Recharge by direct rainfall infiltration occurs throughout the Atherton Tablelands and groundwater discharges as springs and as baseflow within streams (Cook et al. 2001). Hydraulic conductivity values for the basalt aquifer system vary from 0.1 to 104 m/day and specific yields from 1 to 20%, with an average specific yield of 6.4% (Pearce and Durick 2002).

The basalt sequence is underlain by granitic and metamorphic basement rocks, from which smaller groundwater supplies are also obtained, particularly in the south-eastern part of the study area. The hydrogeology of the Atherton Tablelands region is discussed by Leach (1986), Bean (1999), Cook et al. (2001), Herczeg (2001), Pearce (2002) and Pearce and Durick (2002).

5 Hydrogeochemistry

The basalt groundwaters of the Atherton Tablelands may be characterized as follows (Locsey and Cox 2000, 2002a; Herczeg 2001):

- low salinity waters with electrical conductivities ranging from 26 to 460 μS/cm, with most samples less than 250 μS/cm;
- mostly neutral to alkaline waters with pH values from 5.4 to 9.4, although most samples have pH values ranging from 6.5 to 8.5;
- the major dissolved constituents are silica and HCO_3^-, with average concentrations of SiO_2 and HCO_3^- of 93 and 83 mg/L, respectively (dissolved silica in the Atherton Tablelands groundwaters is most likely present in the form H_4SiO_4 given the range of pH values, although silica is also referred to here as SiO_2); and
- low concentrations of Cl^- and SO_4^{2-}, generally less than 15 and 10 mg/L, respectively.

6 Methods

6.1 Mineralogical

Samples to be analyzed by XRD were dried, crushed and micronized (<2 μm), and prepared as 1.5–2 g random powder sample mounts in the manner described by Bish and Post (1989). Mineral composition of basalt and basement material was determined using XRD (a Philips PW 1050 diffractometer equipped with a cobalt anticathode). This is a widely used technique for mineral identification, particularly for fine-grained materials where the grain size is too small to be usefully studied with the optical microscope. Samples were scanned from $2\theta = 2°–76°$. The identification and quantification of mineral phases was assisted by computer programs such as Jade (a search-match program) and Siroquant (a quantification program that expresses the composition of crystalline material within a

sample in percentages of dry weight). An internal standard (10% corundum) was also added to the samples to enable the estimation of the amount of amorphous material.

The program Jade searches a large database of mineral XRD intensity patterns and matches those ideal patterns with the experimental ones. The limitation of this search-match process is that similar crystallographic structures result in similar XRD patterns, and this can make mineral identification questionable, especially of minerals belonging to the same series such as plagioclase feldspars or pyroxenes.

The Siroquant program provides quantitative analyses of mineral phases based on the principle of Rietveld analysis (pattern synthesis) (Reitveld 1969); an ideal XRD pattern is synthesized from basic crystal structure data for each mineral in the sample. These synthesized patterns are added and fitted by a least squares refinement to the sample pattern. The quantification of the experimental XRD trace is thus indirectly performed by quantifying the synthesized pattern. There is rarely a perfect fit between a calculated (synthesized) pattern and the observed (experimental) one; this imperfect fit results in errors in the quantification of each mineral phase. Chi-squared values are obtained as a measure of the "goodness of fit" between theoretical and measured traces from which absolute errors for the weight percentages of each phase are calculated. In this study, the average phase error is $\pm 1\%$ (87% of the samples analyzed have a phase error $<\pm 2\%$); these error values are of a similar order to those obtained by Phillipo et al. (1997) and Hill et al. (2000) using Siroquant.

The XRD mineral identification and quantification procedure used in this study has been assessed by comparing the XRD results with major element geochemistry data provided by Sheldrick (1999), which was used to calculate the mineral norm in the manner described by Faure (1998).

6.2 Hydrochemical

The hydrogeochemical basis for this study is a large set of groundwater analyses obtained from the Queensland Department of Natural Resources and Mines from bores sampled in the Atherton Tablelands region mostly during 1998 and 1999, and additional groundwater analyses from samples collected by the principal author during May and October 1999. The samples were analyzed using inductively coupled plasma optical emission spectroscopy (ICP-OES) for cations, high performance ionic liquid chromatography for chloride and sulfate, and titration with 0.009 N Standard HCl for HCO_3^- and CO_3^{2-}. The ICP-OES was calibrated against appropriate standards and against a blank prepared with nitric acid.

A total of 473 sets of groundwater analyses were used in this study; these samples were collected from bores that were logged as "basalt" or are samples that are characterized by Locsey and Cox (2002a) as having a "basaltic" groundwater composition, an assessment based on the concentrations of the major dissolved constituents.

6.3 Hydrogeochemical Modeling

The program PHREEQC (Parkhurst and Appelo 1999) was used to calculate aqueous speciation values and to assess the state of equilibrium between the groundwaters and primary and secondary minerals. Inverse geochemical modeling was also undertaken using PHREEQC to define possible chemical reactions in the basalt aquifer based on the observed data and to calculate mass transfers of water–rock interactions (Plummer 1992; Nordstrom and Munoz 1994). Based on initial and final water compositions and having defined a net geochemical reaction (i.e., a selected set of reactants and products), a mass

balance was computed based on the change in total molality of the constituents along the reaction path (Plummer and Back 1980). Mass balance calculations are represented as a matrix of simultaneous equations in the manner described by Garrels and Mackenzie (1967) and Wood and Low (1986).

7 Mineralogy of the Atherton Tablelands Basalt Aquifer System

The most abundant primary minerals in basalts are pyroxenes and feldspars (e.g., Nesbitt and Wilson 1992; Gíslason and Arnórsson 1993; Pawar 1993; Pawar et al. 2008; Gíslason et al. 1996; Hill et al. 2000; Edmunds et al. 2002). Pyroxenes have the general formula $X_2Si_2O_6$, in which X is usually Mg, Fe, Mn, Li, Ti, Al, Ca, or Na. The clinopyroxenes diopside and augite are both structurally and chemically similar and may therefore be difficult to distinguish from each other using XRD. The pyroxene phase identified in the Atherton basalts by XRD may be augite with the composition $Ca(Mg, Fe)Si_2O_6$ or $Ca(Fe, Mg)Si_2O_6$, or diopside, a primarily calcium magnesium silicate, with the composition $CaMgSi_2O_6$ or $Ca(Mg, Al)(Si,Al)_2O_6$ (the pyroxene mineral phase present in the Atherton basalts will hereafter be referred to as diopside, although either or both phases may be present). Both diopside and augite have been identified in the Atherton basalts using petrographic microscope and electron microprobe analytical techniques (Sheldrick 1999).

Traces of olivine are also present in some of the Atherton basalt samples. Olivines range continuously in composition from forsterite [Mg_2SiO_4] to fayalite [Fe_2SiO_4]. The olivines identified in these basalts are forsterite and an intermediate phase with the composition $[Mg_{.672}Fe_{.323})_2SiO_4$. As the XRD peaks for diopside [2.991 (1), 2.528 (0.4), 2.893 (0.3)] are similar to those of the olivines fayalite [2.831 (1), 2.501 (0.7), 2.566 (0.5)] and forsterite [2.458 (1), 2.512 (0.7), 3.883 (0.7)], and given that the samples identified are not pure end-members, it can be difficult to distinguish these minerals from each other using XRD.

The feldspar group of minerals have the general formula $X(Al, Si)_4O_8$, in which X is Na, K, Ca, or Ba. The chemistry of the plagioclase feldspars changes progressively from albite (Ab100-90) through oligoclase (Ab90-70), andesine (Ab70-50), labradorite (Ab50-30), bytownite (Ab30-10) to anorthite (An10-0). The plagioclase feldspars identified in the Atherton basalt samples by XRD range from the sodium aluminum silicate albite [$NaAlSi_3O_8$] to the calcium aluminum silicate anorthite [$CaAl_2Si_2O_8$ or $(Ca, Na)(Al, Si)_2Si_2O_8$], and therefore are grouped and reported as "plagioclase feldspars". Analysis of basalt mineral chemistry by Sheldrick (1999) using electron microprobe indicates that the groundmass plagioclase in the alkali olivine basalts and olivine tholeiites ranges from oligoclase to andesine to labradorite, and that the phenocrysts have a labradorite composition.

K-feldspars have been identified in the Atherton basalts by XRD, although it is difficult to identify the phases present, which may include sanidine (a high temperature form of K-feldspar, which may occur as phenocrysts in volcanic rocks), orthoclase, microcline, or anorthoclase. Sanidine, for example, is present in basalts from eastern New South Wales (Craig and Loughnan 1964) and basalts from Mexico City (Edmunds et al. 2002). Minor quartz [SiO_2] is also present in some of the Atherton basalt samples. Microcrystalline silica is commonly observed as a precipitate in vesicles in basalt (e.g., Craig and Loughnan 1964; Wood and Low 1986). Quartz and muscovites with the composition $KAl_2Si_3AlO_{10}(OH)_2$, $KMg_3AlSi_3O_{10}(OH)_2$ (phlogopite), or $(K, Na)Al_2(SiAl)_4O_{10}(OH)_2$, in addition to plagioclase and K-feldspar, are significant components of the basement rocks.

Clay minerals present in the Atherton basalt samples are those of the kaolinite group [$Al_2Si_2O_5(OH)_4$] and the smectites, which may be montmorillonite [$Ca_{0.2}(Al, Mg)_2Si_4O_{10}(OH)_{2.4}H_2O$] or the Fe-smectite nontronite [$Na_{0.3}Fe_2Si_4O_{10}(OH)_{2.4}H_2O$]. Nontronite has also been observed in basalt, as a weathering product of labradorite in the eastern Snake River Plain basalts for example (Wood and Low 1986); smectite and kaolinite minerals are the dominant weathering products of basalts from eastern New South Wales (Craig and Loughnan 1964), basalts north-northwest of Melbourne (Nesbitt and Wilson 1992), and basalts in central and southern Portugal (Prudêncio et al. 2002). The Atherton Tablelands basement rock samples, of granite and diorite composition, have minor kaolinite and smectite, chlorite [$(Mg, Fe, Al)_6(Si, Al)_4O_{10}(OH)_8$] and possibly illite [$KAl_2(Si_3Al)O_{10}(OH)_2$], the latter two being weathering products of micas.

Accessory minerals observed in the Atherton basalt samples include gibbsite [$Al(OH)_3$], hematite [Fe_2O_3], goethite [FeO(OH)], and siderite[$FeCO_3$], which occur as secondary product in vesicles or along fractures in basalt or as nodules in clays. Hematite and goethite are also observed as accessory minerals in basalts in Portgual (Prudêncio et al. 2002), while gibbsite, siderite and iron oxides, and oxyhydroxides commonly infill vesicles in the basalts of the Kerikeri area of North Auckland (Carr et al. 1980). Minor pyrite [FeS_2] is also observed in many of the Atherton basalt samples; hypogene pyrite can be found replacing magnetite and ferromagnesian minerals in basalt.

Other minerals present in the basalt samples include the feldspathoids nepheline [$K(Na, K)_3Al_4Si_4O_{16}$] and analcime [$NaAlSi_2O_6.H_2O$]. Analcime can also be classed as a zeolite mineral, which may form as a weathering product of volcanic ash. Analcime may be present as a primary mineral in some basalts occurring as phenocrysts or in the groundmass (Deer et al. 1966; Liou 1971) and is also a common secondary mineral in basalt at low temperatures (<50°C) (White et al. 1980; Arnórsson 1999; Prudêncio et al. 2002). The zeolites chabazite [$CaAlSi_4O_{12}.6H_2O$] that may occur in cavities in basalt (Hamilton et al. 1989; Tschernich 1992) and a phase identified as either gottardiite [$Na_3Mg_3Ca_5Al_{19}Si_{117}O_{272}.93H_2O$] or boggsite [$NaCa_2(Al_5Si_{19}O_{48}).17H_2O$] are common accessory minerals in the Atherton basalt samples. Gottardiite and boggsite, in addition to a variety of other zeolite minerals, have also been identified in basalts from cold climates such as Mount Adamson, Antarctica (Galli et al. 1995, 1996; Alberti et al. 1996) and boggsite in basalts from Goble, Oregon (Howard et al. 1990). Other zeolite minerals present in the Atherton basalt samples include natrolite [$Na_2Al_2Si_3O_{10}.2H_2O$] and laumontite [$CaAl_2Si_4O_{12}.4H_2O$], which occur in veins and cavities of igneous rocks.

Zeolites such as analcime, chabazite, laumontite, and many others, in addition to pyrite, calcite, dolomite, sepiolite, quartz, and clay minerals have been identified as alteration products of the Columbia Plateau basalts, and/or to be in equilibrium with the groundwaters of the Columbia Plateau basalts (Deutsch et al. 1982). A variety of zeolite minerals, including chabazite and natrolite, are also observed in Tertiary basalts in Northern Ireland (Walker 1960; Lyle 1974), Ca-rich zeolites as alteration products in basalts in Iceland (Crovisier et al. 1992), and zeolites, clays, and carbonates in the Deccan basalts around the Pune area in India (Pawar 1993).

Analcime and/or chabazite have been identified in many Australian basaltic rocks, such as the Tertiary basalts at Clermont, Killarney, and Warwick in Queensland, the Newer Volcanics basalts in Victoria, Tertiary basalts at Mount Bell in Tasmania, and the Garrawilla volcanics near Gunnedah in New South Wales (Chalmers 1967; Head 1979).

Other minerals identified in the Atherton basalts by Sheldrick (1999), although not identified during XRD analyses, include ilmenite, titano-magnetite, Cr-spinel, and apatite. Apatite has also been observed in small quantities in the Tertiary basalts of the Baynton

Fig. 2 **a–c** XRD traces for three basalt samples from bore 11000133 at 8 m (highly weathered basalt or saprolite), 19 m (relatively fresh basalt), and 56 m (weathered basalt containing secondary minerals), showing the significant mineral phases identified in each sample. *Y* axes, representing the number of X rays measured in a given peak, are at different scales

profile north–north-west of Melbourne (Nesbitt and Wilson 1992) and in the Tertiary basalts of Northern Ireland (Hill et al. 2000) and Mexico City (Edmunds et al. 2002), and magnetite as an accessory mineral in basalts in Portugal (Prudêncio et al. 2002). The amount of amorphous material in the Atherton samples was estimated through the use of corundum (Al_2O_3) as an internal standard. Amorphous material may be present as glassy material, charcoal in palaeosols, or organic matter.

XRD traces for three basalt samples from bore 10000133 are presented in Fig. 2, showing the significant mineral phases identified in each sample. Figure 2a from basalt sampled at a depth of 8 m is an example of highly weathered basalt or saprolite, dominated by clay (kaolinite) and aluminum and iron oxides (gibbsite and hematite). Figure 2b at 19 m is an example of relatively fresh basalt comprising plagioclase feldspar (mainly anorthite), K-feldspar (possibly orthoclase), pyroxene (diopside), and kaolinite. Figure 2c at 56 m is an example of weathered basalt comprising plagioclase feldspar (mainly anorthite), pyroxene (possibly augite), olivine (fayalite), kaolinite, and secondary quartz, hematite, and pyrite.

Results of quantitative XRD analyses of mineral phases for selected drill chip samples from bores 11000128, 11000136, and 11000133 are presented in Tables 1, 2, and 3, and in diagrammatic form in Fig. 3. The mineralogy of the three profiles is discussed below, followed by a summary of the mineralogical observations, including in relation to groundwater occurrence and composition.

7.1 Mineralogical Profiles

7.1.1 11000128

Most of the basalt sequence intersected by bore 11000128 (i.e., 39–82 m) is dominated by primary minerals, those being, pyroxenes, plagioclase feldspars, and K-feldspar, with an average of only 11% clay minerals (kaolinite and smectite). Fresh granite is observed at the base of the profile (89 m), comprising 47% quartz, 28.8 and 11.1% plagioclase feldspars and K-feldspar, respectively, 10% muscovite, and a small percentage of clay minerals (2.7%). Immediately above the granite basement (85 m), the sample is comprised of clays (46%), quartz (26%), plagioclase feldspars (13.1%), pyroxenes (12.2%), and K-feldspar (2.7%). This is interpreted to be a mixture of weathered granite and the base of the basalt pile. The upper part of the profile (samples at 6 and 19 m) is dominated by kaolinite at 86.9 and 73.3% for these samples, respectively. Fresher basaltic material is present below this at 23 and 32 m, with near equal amounts of kaolinite and smectite clays. The dominance of kaolinite over smectite content in the upper layers indicates that kaolinite is the residual product of the destruction of smectite, as also observed for some basic volcanic rock profiles in eastern New South Wales (Craig and Loughnan 1964).

The average amorphous content of the basalt samples is 3.7%, which is likely to be organic matter and glassy material, in addition to a small percentage of unidentified mineral phases. Accessory minerals such as hematite and siderite are present throughout the basalt sequence, and traces of pyrite and the zeolite chabazite occur in some basalt samples. The zeolite mineral inferred to be gottardiite (or boggsite) is present in amounts

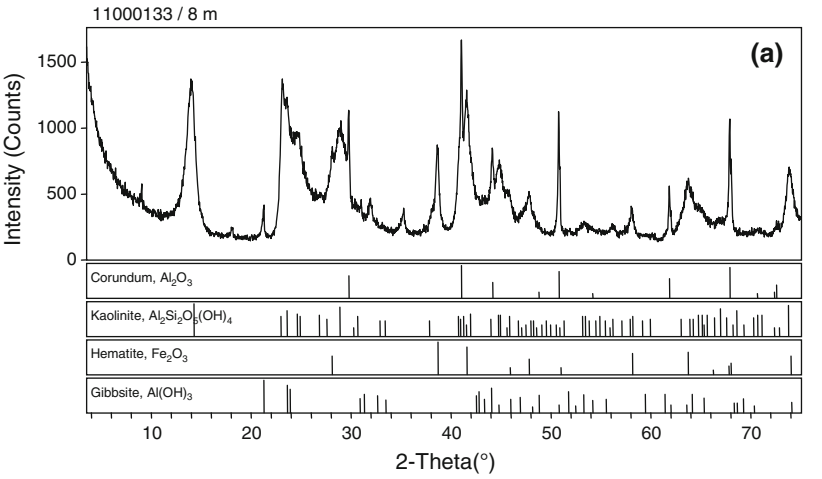
11000133 / 8 m
(a)
Intensity (Counts)
1500
1000
500
0
Corundum, Al_2O_3
Kaolinite, $Al_2Si_2O_5(OH)_4$
Hematite, Fe_2O_3
Gibbsite, $Al(OH)_3$
10
20
30
40
50
60
70
2-Theta(°)

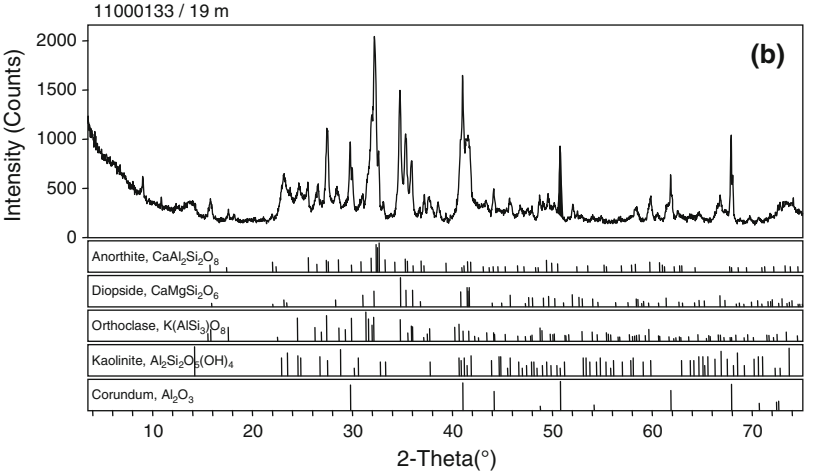
11000133 / 19 m
(b)
Intensity (Counts)
2000
1500
1000
500
0
Anorthite, $CaAl_2Si_2O_8$
Diopside, $CaMgSi_2O_6$
Orthoclase, $K(AlSi_3)O_8$
Kaolinite, $Al_2Si_2O_5(OH)_4$
Corundum, Al_2O_3
10
20
30
40
50
60
70
2-Theta(°)

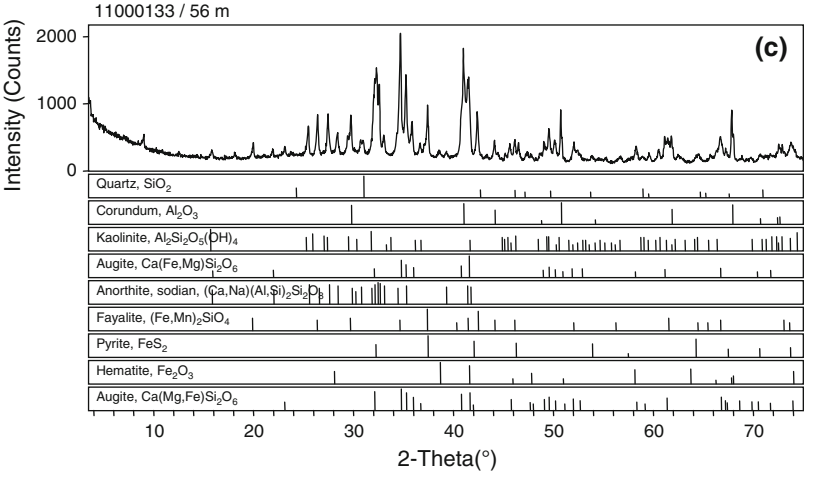
11000133 / 56 m
(c)
Intensity (Counts)
2000
1000
0
Quartz, SiO_2
Corundum, Al_2O_3
Kaolinite, $Al_2Si_2O_5(OH)_4$
Augite, $Ca(Fe,Mg)Si_2O_6$
Anorthite, sodian, $(Ca,Na)(Al,Si)_2Si_2O_8$
Fayalite, $(Fe,Mn)_2SiO_4$
Pyrite, FeS_2
Hematite, Fe_2O_3
Augite, $Ca(Mg,Fe)Si_2O_6$
10
20
30
40
50
60
70
2-Theta(°)

Table 1 Results of selected XRD quantitative analyses of mineral phases for samples from bore 11000128 (results expressed as wt%)

Bore/sample depth	Pyroxenes[a]	Plagioclase	K-feldspar	Kaolinite	Smectite	Quartz	Muscovite	Others[b]
11000128/6 m	4.0	4.2	1.7	86.9	1.1	0.9	0.0	1.1(Gd)
11000128/19 m	2.9	9.4	8.5	73.3	1.8	1.4	0.0	2.8(H, Gd, P)
11000128/32 m	13.1	33.9	10.3	17.8	20.0	0.6	0.0	4.2(H, Gd, C, S)
11000128/50 m	30.6	51.2	11.3	2.7	0.7	0.6	0.0	2.9(H, Gd, S)
11000128/58 m[c]	67.3	3.7	5.0	6.9	8.5	0.0	0.0	8.0(Gt, Gb, Gd, H, S, P)
11000128/65 m	39.3	36.4	8.2	3.2	8.8	0.6	0.0	3.5(Gd, H, Gt, S)
11000128/82 m	39.4	40.2	4.3	10.2	3.2	Traces	0.0	2.7(Gd, S, H)
11000128/85 m	12.2	13.1	2.7	16.8	29.2	26.0	0.0	0.0
11000128/89 m	0.0	28.8	11.1	2.3	0.4	47.0	10.3	0.0

[a] Diopside and/or augite

[b] Hematite (H), siderite (S), goethite (Gt), gibbsite (Gb), pyrite (P), chlorite (Ch), and zeolites such as gottardiite/boggsite (Gd) and chabazite (C), listed in order of decreasing abundance

[c] Approximate values as sample also contains small amounts of analcime, which is unquantified

Table 2 Results of selected XRD quantitative analyses of mineral phases for samples from bore 11000133 (results expressed as wt%)

Bore/sample depth	Pyroxenes[a]	Plagioclase	K-feldspar	Kaolinite	Smectite	Quartz	Muscovite	Others[b]
11000133/8 m	2.2	1.7	1.2	71.4	0.0	0.0	0.0	23.4(H, Gb)
11000133/19 m	17.7	27.6	18.5	26.6	1.4	Traces	0.0	8.2(C, Gd, H, S, P)
11000133/25 m	27.9	33.1	10.1	19.8	Traces	Traces	0.0	9.1(C, H, Gd, P)
11000133/36 m	29.1	48.8	10.0	7.5	0.8	Traces	0.0	3.8(S, Gd)
11000133/50 m	27.8	42.3	11.8	12.7	Traces	Traces	0.0	5.3(C, Gd, S, H, P)
11000133/54 m (zeolite)	4.5	22.7	4.9	55.6	5.3	1.3	0.0	5.7(S, C, Gd)
11000133/54 m	9.4	47.9	18.2	16.9	5.2	1.1	0.0	1.1(Gd)
11000133/56 m	6.7[c]	29.0	14.0	36.7	6.4	1.3	0.0	5.9(H, C, Gd, P)
11000133/60 m	5.7	32.2	14.9	34.0	10.3	Traces	0.0	2.9(H, Gd, C, P)

Sample 11000133/54 m (zeolite) was selectively sampled to determine zeolite phases clearly observed in hand specimens

[a] Diopside and/or augite

[b] Hematite (H), siderite (S), goethite (Gt), gibbsite (Gb), pyrite (P), chlorite (Ch), and zeolites such as gottardiite/boggsite (Gd) and chabazite (C), listed in order of decreasing abundance

[c] Includes traces of olivine

Table 3 Results of selected XRD quantitative analyses of mineral phases for samples from bore 11000136 (results expressed as wt%)

Bore/sample depth	Pyroxenes[a]	Plagioclase	K-feldspar	Kaolinite	Smectite	Quartz	Muscovite	Others[b]
11000136/16 m	5.3	25.6	9.4	43.7	12.5	1.3	0.0	2.2(Gd, C, S, P)
11000136/29 m	10.8	41.4	12.5	23.5	9.6	Traces	0.0	2.1(Gd)
11000136/33 m	0.0	6.1	2.7	61.8	2.6	21.5	0.0	5.4(H, Gd)
11000136/42 m	2.6	16.1	9.1	30.1	39.5	0.6	0.0	2.0(Gd)
11000136/54 m	7.0	29.1	11.0	11.8	36.7	1.2	0.0	3.2(Gd, H, P)
11000136/60 m	19.7	33.7	10.2	18.9	14.4	1.5	0.0	1.7(Gd, C)
11000136/69 m	8.4	10.3	4.9	37.1	34.8	1.2	0.0	3.1(Gd, C, S, H, P)
11000136/79 m	38.5	40.9	6.9	4.2	2.0	1.7	0.0	5.8(Gd, H, S, P)
11000136/86 m	22.4	19.1	3.3	23.5	7.1	5.9	18.8	0.0
11000136/91 m	0.0	31.0	0.0	8.5	0.2	6.5	47.5	6.3(Ch)

[a] Diopside and/or augite

[b] Hematite (H), siderite (S), goethite (Gt), gibbsite (Gb), pyrite (P), chlorite (Ch), and zeolites such as gottardiite/boggsite (Gd) and chabazite (C), listed in order of decreasing abundance

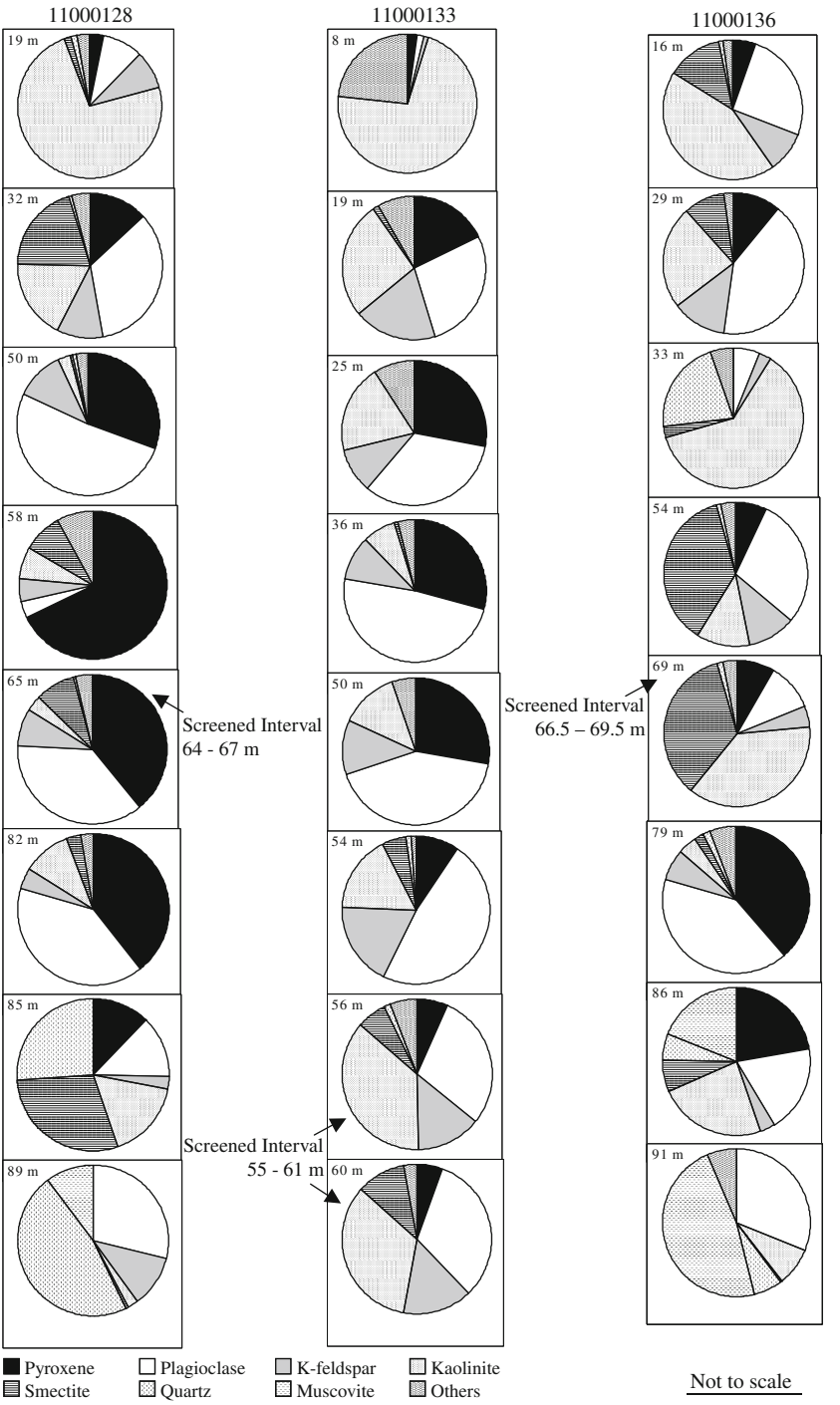

Fig. 3 Quantification of mineral phases present in selected drill chip samples from groundwater bores 11000128, 11000133, and 11000136

from 1 to 2% throughout the basalt profile, although the 11.3 Å peak in the d spacing for this mineral is sharpest in the fresher basalt; analcime is present in the fresh, pyroxene-dominated samples at 58 and 59 m. Zeolite minerals were also observed by Buck (1999) throughout much of this basalt profile. Sharper zeolite peaks in the fresher basalt may indicate that, although these zeolites are likely to be weathering products, they may be better preserved in the fresher, rather than in the more weathered basalt material. Phenocrysts of fresh and weathered olivine were also observed throughout the basalt profile by Buck (1999); however, olivine was not quantified from the XRD analyses of samples from this profile. This may be because of its occurrence as only a very small percentage of the whole rock composition, or because of the difficulty in distinguishing olivine minerals from pyroxenes such as diopside using XRD.

Goethite and gibbsite are present in the predominantly fresh basalt samples from 52 to 74 m. The greatest percentages of goethite (2.6–3.2%) and gibbsite (1.8–2.6%) occur in the samples at 58 and 59 m, which have the greatest amounts of pyroxene (67.3 and 71%) in this basalt profile and are described by Buck (1999) as massive lavas with minor vesicles. Buck (1999) also observed that the secondary minerals in these samples have a platey character. These Fe and Al weathering products are interpreted to be weathering products of the pyroxenes that occur along fractures in the basalt. As the most significant zone of groundwater flow in the bore, from 64 to 67 m, is just below the samples discussed above, it may be inferred that the Fe and Al weathering products are actively forming and that the fractures in these basalts are an important pathway for groundwater movement.

7.1.2 11000136

The basalt samples from 16 to 79 m of bore 11000136 are comprised of the primary minerals pyroxenes (2.6–38.5%), plagioclase feldspars (6.1–45.2%), K-feldspar (2.7–12.5%), quartz (mostly <1.7%, although the sample at 33 m has 21.5% quartz), gottardiite up to 2% throughout the basalt profile, traces of pyrite and chabazite, siderite and hematite up to 1.8 and 3.4%, respectively, and an average amorphous content of 2.6%. The mineralogy of the samples from bore 11000136 indicate a thick sequence (to depths between 79 and 86 m) of basalt lava flows that show variable degrees of weathering, with clay contents mostly 31–72%, with fresher basalt at 79 m (containing 6.3% clays). The relative degrees of weathering are probably related to the time of exposure of the tops of the lava flows prior to burial by subsequent lava flows.

The clay contents of the basalt samples from bore 11000136 are considerably higher than for most of the basalt sequence intersected by bore 11000128, indicating that the lava flows in the area intersected by bore 11000136 were exposed to weathering at the surface for longer periods than the lava flows in the area of bore 11000128. As bore 11000136 is located to the north of bore 11000128, and the lava sources (the Atherton Volcano and Bones Knob) were located to the south and east–south-east of bore 11000128, with lava flowing northwards (Bean 1999) (Fig. 1), it is likely that not all of the lava flows reached the area of bore 11000136. This would have allowed for a longer period of weathering between the emplacement of lava flows, and for the development of palaeosols, such as that observed at 33 m, which has a high kaolinite (61.8%) and quartz (21.5%) content. From depths of 42–69 m, the smectite content is approximately equal to or greater than the kaolinite content, which may indicate a lower rainfall at the time of the weathering of these basalt layers than at present, and poorer drainage conditions.

The screened interval (66.5–69.5 m) of bore 11000136 is located in highly weathered basalt, with a clay content of approximately 71%, indicating that the groundwater tends to

occur in highly weathered basalt between fresher basalt layers such as at 79 m (pyroxene + plagioclase feldspars = 79.4%) and 60 m (pyroxene + plagioclase feldspars = 53.4%). The groundwater obtained from bore 11000136 has some of the highest concentrations of Fe^{2+} and Al^{3+} of the groundwaters in the region, with average concentrations of 1.3 and 1.6 mg/L, respectively. This may be due to interaction with clays in the highly weathered basalt within which the groundwater is stored. The Na^{+} concentrations of the groundwater sampled from bore 11000136 are also particularly high for this area (with an average of 42 mg/L), which may indicate a process of ion-exchange between the groundwater and the clay minerals, with Na^{+} released to solution.

The sample at the base of the profile (91 m) is predominantly muscovite (47.5%) and plagioclase feldspar (31%), with smaller amounts of quartz (6.5%) and the clay minerals kaolinite (8.5%) and chlorite (6.3%). This basement rock is identified by Bean (1999) as Early Permian Tinaroo Granite. However, the low quartz content of the basement rock indicates a composition approximating diorite, and the presence of chlorite, in addition to kaolinite, may be the result of chloritization of muscovite. The sample at 86 m is interpreted to be a mixture of weathered diorite and basalt.

7.1.3 11000133

The uppermost part of the basalt profile sampled from bore 11000133 at 8 m is dominated by weathering products, that is, kaolinite (71.4%) and hematite (22%), with minor gibbsite (1.4%). The basalt profile beneath this highly weathered upper layer may be interpreted as representing a number of basalt flows within two distinct events. The upper, younger event, extending to a depth of approximately 50 m, has an average plagioclase feldspar content of 54%, an average pyroxene content of 25.5%, and clays from 8.3 to 28%, which are mostly kaolinite, with smectite comprising <2.1% of the whole rock composition, and traces of quartz. The upper event may be regarded as a relatively fresh sequence of basaltic rocks.

The lower, older event, extending from 54 m to at least the base of the bore at 60 m, has a similar average plagioclase feldspar content of 50%, but considerably lower pyroxene (average of 7%) and a higher clay content (22.1–44.8%), which includes a higher smectite content of 5.2–10.3%. The quartz content in the lower basalts is also slightly higher from trace amounts to 1.5%. The basalts in the lower part of the profile of bore 11000133 are significantly more weathered than the basalts above 50 m.

The K-feldspar content is reasonably consistent throughout the basalt profile, with an average of 13.4% (excluding the uppermost weathered sample). Weathering products such as hematite (up to 3.4%), siderite (up to 2.5%), and traces of pyrite are also present throughout the basalt profile, in addition to the zeolites chabazite (up to 3.6%) and gottardiite (up to 2.9%). Traces of olivine are also present in the sample taken at 56 m, and the average amorphous content is 2.6%.

The variations in the mineralogical content of this profile indicate that the basalts described in the lower event have undergone more prolonged weathering than the overlying basalts, resulting in the preferential weathering of pyroxenes to kaolinite and smectite clays. The geological log for this bore (provided by the Queensland Department of Natural Resources and Mines) indicates that the upper basalts are massive with some fracturing and that the lower basalts are more vesicular. The screened interval of this groundwater bore is from 55 to 61 m and is located in the more weathered layers of the older event, indicating that the groundwater is stored in the vesicular and more weathered lower basalts, and that the fractures in the fresher and massive overlying basalts may be important recharge pathways.

7.1.4 Summary

The three basalt profiles discussed above show considerable variation in mineralogical content and degree of weathering, indicating that the rocks of the Atherton Tablelands comprise a very heterogeneous sequence of basaltic material, including several flow events overlying older basement rocks.

The type of clay minerals formed during weathering is related to the water composition (e.g., kaolinite is formed in dilute waters and smectites are formed in more concentrated solutions), which is connected to the rainfall amount (Berner 1971; Drever 1997). The occurrence of a relatively high smectite content in some of the highly weathered basalt layers (e.g., 11000136/42–60 m) may indicate considerably lower levels of precipitation at the time of lava exposure and weathering, and relatively poorer drainage conditions than at present. The relationship between the relative clay mineral contents and mean annual precipitation for basic igneous rocks in California was observed by Barshad (1966). At a rainfall of approximately 500 mm/yr, the percentage of smectite and kaolinite/halloysite in the surface layers of residual soils is roughly equal; with increasing precipitation, the relative kaolinite/halloysite content increases and the smectite content decreases substantially; the reverse was observed with decreasing rainfall (Barshad 1966). Based on the current rainfall in the Atherton Tablelands region, the weathering of silicate minerals to kaolinite clays should prevail over smectite formation.

Groundwater in the basalts may occur in both vesicular and fractured rock, and the degree of weathering may influence the storage capacity. The total pile of the Atherton basalts is regarded as behaving as an unconfined aquifer system (Pearce 2002), with recharge occurring locally (Bean 1999). While the horizontal hydraulic conductivity is probably greater than the vertical hydraulic conductivity, the work presented here indicates that, while groundwater is more likely to be stored within fresh or weathered vesicular layers (including palaeosols), fractures are important pathways for groundwater movement in this aquifer system. The importance of fractures in terms of recharge to and movement of groundwater through basalt aquifer systems has also been noted by Ecker (1976).

8 Major Element Geochemistry

The identification of minerals with similar crystallographic structures, such as minerals in the pyroxene and plagioclase feldspar series, can be difficult using XRD techniques as noted above. As a means of examining the reliability of the XRD results, the data may be compared to the calculated abundances of selected minerals from chemical analyses of the rocks. The resulting mineral composition (the norm) from such calculations is comprised of selected normative minerals. The procedure for calculating a mineral norm, outlined by Faure (1998), was applied to this study.

Major element geochemistry data for the Atherton Tablelands basalts are provided by Sheldrick (1999). Average major element geochemistry data, based on 34 fresh drill chip samples from alkali olivine basalts, basanites, and olivine tholeiites, expressed as a percentage of the rock and in millimoles/100 g of fresh basalt are presented in Table 4, as well as the calculation of the mineral norm. These basalts generally belong to the high TiO_2 type ($TiO_2 > 2\%$) (Benedetti et al. 1994) with TiO_2 ranging from 1.71 to 2.67% and an average of 2.05%.

The major element geochemistry data for these samples are comparable to other provinces in eastern Australia, such as the Newer Volcanics basalts in Victoria (Price et al. 1997),

Table 4 Average major element geochemistry data based on 34 fresh drill chip samples from alkali olivine basalts, basanites, and olivine tholeiites (after Sheldrick 1999) and calculation of a mineral norm

Fresh basalt	SiO_2	Al_2O_3	CaO	MgO	Na_2O	K_2O	Fe_2O_3	MnO	TiO_2	P_2O_5	LOI	
%	47.61	14.25	9.06	8.18	3.07	1.66	11.49	0.16	2.05	0.59	1.81	
mmol/100 g	792	140	162	203	49.6	17.6	71.9	2.31	25.7	4.15	101	
Minerals	*Millimoles/100 g*											*Normative minerals (%)*
$K_2O{\cdot}Al_2O_3{\cdot}6SiO_2$ K-feldspar	686	122.4	162	203	49.6	0	71.9	2.31	25.7	4.15	101	9.80
$Na_2O{\cdot}Al_2O_3{\cdot}6SiO_2$ Albite	506	92.4	162	203	19.6	0	71.9	2.31	25.7	4.15	101	15.7
$CaO{\cdot}Al_2O_3{\cdot}2SiO_2$ Anorthite	386	32.4	102	203	19.6	0	71.9	2.31	25.7	4.15	101	16.7
$CaO{\cdot}MgO{\cdot}2SiO_2$ Diopside	207	32.4	12.45	113.5	19.6	0	71.9	2.31	25.7	4.15	101	19.4
$2MgO{\cdot}SiO_2$ Olivine (forsterite)	151	32.4	12.45	0	19.6	0	71.9	2.31	25.7	4.15	101	16.0
$Al_2O_3{\cdot}2SiO_2{\cdot}2H_2O$ Kaolinite	118.2	16.2	12.45	0	19.6	0	71.9	2.31	25.7	4.15	68.6	4.18
$Na_2O{\cdot}Al_2O_3{\cdot}2SiO_2$ Nepheline	85.8	0	12.45	0	3.4	0	71.9	2.31	25.7	4.15	68.6	4.60
$FeO{\cdot}TiO_2$ Ilmenite	85.8	0	12.45	0	3.4	0	12.9	2.31	0	4.15	68.6	3.90
Fe_2O_3 Hematite	85.8	0	12.45	0	3.4	0	0	2.31	0	4.15	68.6	2.05
MnO_2 Pyrolusite	85.8	0	12.45	0	3.4	0	0	0	0	4.15	68.6	0.20
$3CaO{\cdot}P_2O_5$ Apatite	85.8	0	0	0	3.4	0	0	0	0	0	68.6	0.82

Table 4 continued

Fresh basalt	SiO_2	Al_2O_3	CaO	MgO	Na_2O	K_2O	Fe_2O_3	MnO	TiO_2	P_2O_5	LOI	
%	47.61	14.25	9.06	8.18	3.07	1.66	11.49	0.16	2.05	0.59	1.81	
mmol/100 g	792	140	162	203	49.6	17.6	71.9	2.31	25.7	4.15	101	
SiO_2 Silica	0	0	0	0	3.4	0	0	0	0	0	68.6	5.16
H_2O Water	0	0	0	0	3.4	0	0	0	0	0	0	1.24
											Total	99.74

Total Fe is reported as Fe_2O_3

and are generally comparable to the Tertiary basalts at Baynton in Victoria, those near Carool in northern New South Wales, and the Monaro basalts of southern New South Wales (Eggleton et al. 1987), all occurring in colder climates than the study area. However, the Atherton basalts are slightly enriched in CaO and Na_2O in comparison to the Baynton, Carool, and Monaro basalts. The Atherton basalts also have a similar major elemental composition to the olivine basalts of the Snake River Group, Idaho (Wood and Low 1986) (although the Atherton basalts have 10–15% more MgO and Na_2O and up to 55% more K_2O than those basalts), and a similar major elemental composition to basalts from the Columbia Plateau, Hawaii, and Iceland as quoted by Bluth and Kump (1994) (although the Atherton basalt are also enriched in MgO and K_2O in comparison to those basalts).

The primary minerals selected for the mineral norm calculations are K-feldspar, albite, anorthite, diopside, and olivine (forsterite), the secondary minerals kaolinite and nepheline, and accessory minerals hematite, ilmenite, pyrolusite, and silica. The calculated mineral norm is compared to the XRD results of some fresh basalt samples. An average fresh basalt mineral composition (XRD results) based on the three freshest basalt samples (11000128/50, 11000133/36, and 11000136/79 m) is 32.8% pyroxenes, 15.7% albite, 31.3% anorthite, 9.4% kaolinite, 1.2% hematite, 1.2% smectite, 1.1% quartz, and 1.9% siderite.

The formulae of the minerals in Table 4 are expressed in oxide form, and LOI was assumed to be H_2O. All of the available K_2O was converted into K-feldspar, most of the Na_2O into albite, some of the CaO into anorthite, some of the CaO and MgO into the pyroxene diopside and the remaining MgO into the olivine forsterite, with Al_2O_3 and SiO_2 reduced accordingly for these minerals. A small amount of kaolinite was constructed using Al_2O_3 and proportionate amounts of SiO_2 and H_2O (LOI), and a small amount of nepheline was constructed using Na_2O, Al_2O_3 and SiO_2. All the available TiO_2 was converted into ilmenite and the remaining Fe_2O_3 into hematite. All of the MnO in the analysis was assigned to pyrolusite, and P_2O_5 (and a proportionate amount of CaO) to apatite. The remaining SiO_2 was converted into secondary amorphous or crystalline silica, and the remaining H_2O was converted into water, which coats the solid particles. The sum of the normative minerals is 99.74%.

The calculations presented in Table 4 show that the normative mineral composition is very similar to that obtained by XRD analyses. The pyroxenes identified using XRD are predominantly diopside; however, the mineral norm indicates that the mafic mineral phases are likely to be a combination of diopside and olivine. This dissimilarity is most likely due to the difficulties in distinguishing these minerals from each other using XRD as discussed above. The major element geochemistry data and the calculated mineral norm, do, however, strongly support the XRD mineral identification and quantification procedures used in this study.

9 Hydrogeochemical Processes

In a thermodynamic sense, weathering systems are open, irreversible, and incongruent; weathering reactions are irreversible because they take place primarily as a result of disequilibria between the rocks and their physico-chemical conditions and are incongruent because the dissolved ions are removed by flowing groundwater, while the remaining solid phases differ from the initial solid phases (Middelburg et al. 1988). The effects of weathering processes on the compositions of the Atherton Tablelands and other basalt groundwaters are discussed below.

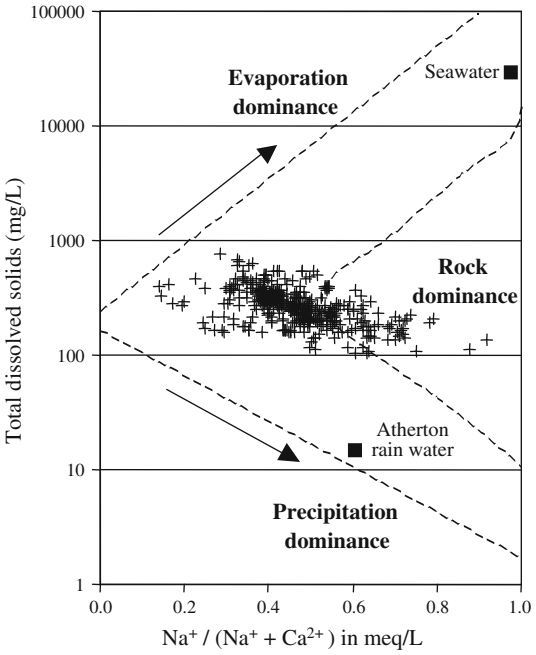

Fig. 4 Variation of the weight ratio of $Na^+/(Na^+ + Ca^{2+})$ as a function of total dissolved solids (TDS) (after Gibbs 1970)

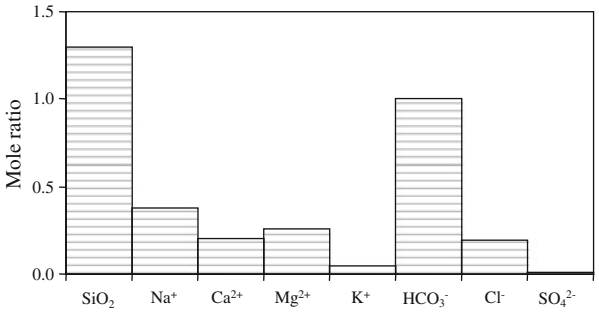

Fig. 5 Average composition of the Atherton basalt groundwaters (based on 473 samples). Heights of the *bars* are proportional to the mole ratio of the constituents relative to HCO_3^-

The source of the major ions in the Atherton basalt groundwaters can be defined by plotting the data according to the variation of the weight ratio of $Na^+/(Na^+ + Ca^{2+})$ as a function of total dissolved solids (Gibbs 1970). On the Gibbs diagram shown in Fig. 4, the data indicate that the major control on the water composition is rock weathering.

The average composition of the Atherton basalt groundwaters is shown in Fig. 5 as mole ratios of the major constituents relative to HCO_3^-. The Atherton basalt groundwaters have considerably higher concentrations of SiO_2 relative to HCO_3^- and, slightly higher Na^+ relative to Ca^{2+} and Mg^{2+} than the basalt groundwaters from Washington and Oregon presented by Garrels (1967) for example. The Atherton basalt groundwaters also have considerably lower concentrations of all the major ions (expect for K^+ which is similar) than both pre- and post-monsoon basalt groundwaters of the Pune area of India (Pawar 1993; Pawar et al. 2008). This is probably due to the higher annual rainfall in the Atherton Tablelands region in comparison to the Pune area. Despite the freshness of the Atherton

basalt groundwaters, the effects of mineral weathering can be observed on the compositions of these groundwaters.

9.1 Mineral Weathering

The aqueous geochemistry data were interpreted using a simplified mass balance technique presented by Hounslow (1995) based on the work of Garrels and Mackenzie (1967). The Atherton basalt groundwaters show the following trends in concentrations (ions in meq/L and SiO_2 in mmol/L): $Na^+ > Cl^-$, $Ca^{2+} > SO_4^{2-}$, $SiO_2 > HCO_3^-$, and $SiO_2 > 2$ ($Na^+ + K^+ - Cl^-$). These trends are indicative of basaltic weathering processes dominated by the weathering of ferromagnesian minerals.

The influence of silicate mineral weathering on the groundwater composition is supported upon further examination of the aqueous geochemistry. Total dissolved solids are low, values of Cl^-/sum anions (<0.8) are indicative of rock weathering, and values of HCO_3^-/sum anions (mostly >0.8) are indicative of silicate mineral weathering in particular. More than 70% of the groundwater samples have values of $(Na^+ + K^+ - Cl^-)/(Na^+ + K^+ - Cl^- + Ca^{2+})$ ranging from 0.2 to 0.8, which indicate that plagioclase weathering is possible. Most samples have $Na^+/(Na^+ + Cl^-)$, $Ca^{2+}/(Ca^{2+} + SO_4^{2-})$, and $Mg^{2+}/(Ca^{2+} + Mg^{2+})$ values >0.5; the high values for the first and second parameters indicate a source of Na^+ and Ca^{2+}, respectively, such as plagioclase feldspars, and the high value for the third parameter indicates the weathering of ferromagnesian minerals.

An enrichment of Mg^{2+} relative to Ca^{2+} was similarly observed by Edmunds et al. (2002) for the basaltic groundwaters of Mexico City and attributed to the weathering of mafic minerals. The enrichment of Na^+ and to a lesser extent Mg^{2+} relative to Ca^{2+} for basaltic groundwaters in India (and similarly observed for the Atherton groundwaters) is attributed not only to the dissolution of silicate minerals such as augite but also to the precipitation of calcite and dolomite, which act as sinks for Ca^{2+} and Mg^{2+} cations (Pawar 1993).

Plagioclase feldspars comprise a significant proportion of the mineral content of the Atherton basalts, and as a result, the ratio of HCO_3^-/SiO_2 in the groundwaters should be related to the feldspar composition and to the weathering products. Using a diagram presented by Garrels (1967), the ratio of HCO_3^-/SiO_2 is plotted against the concentration of dissolved HCO_3^- (Fig. 6). Because the ratio of HCO_3^-/SiO_2 is fixed for a given

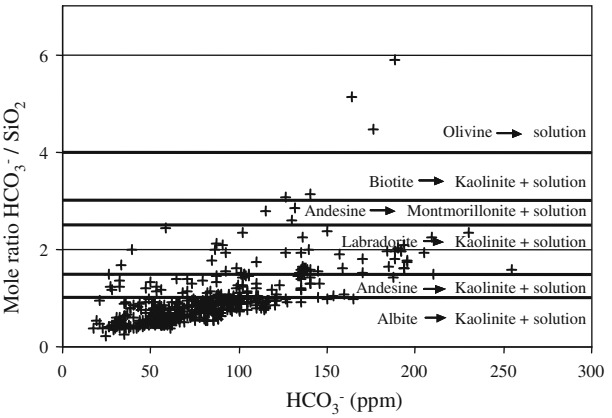

Fig. 6 Mole ratio HCO_3^-/SiO_2 versus ppm HCO_3^- for the Atherton basalt groundwaters. *Horizontal lines* show the HCO_3^- to SiO_2 ratio expected if waters are the result of various reactions for the alteration of primary rock minerals (after Garrels 1967)

weathering reaction involving a given silicate mineral and weathering product, it is possible to indicate the predicted values for the contributions from various rock minerals (Garrels 1967), as shown in Fig. 6. The analytical data indicate that the dominant primary plagioclase feldspar phases probably range from albite to andesine to labradorite and show that kaolinization of the host rocks is likely with HCO_3^-/SiO_2 ratios mostly less than three. Some weathering of plagioclase feldspars to montmorillonite and dissociation of olivine may also occur.

Some of the likely water–rock interactions controlling the concentrations of the major ions in the Atherton basalt groundwaters are the dissociation of olivine, the weathering of pyroxenes (such as augite or diopside) to kaolinite, and the weathering of plagioclase feldspars (such as albite and anorthite) to kaolinite or montmorillonite, with the subsequent release of cations, bicarbonate, and silica to solution (Locsey and Cox 2000, 2002b; Herczeg 2001).

The release of soluble silica by the weathering of aluminosilicates has also been proposed for the sediments of the Tucumán Plain, north-western Argentina. Although the weathering of aluminosilicate minerals is generally slow, in that region the process is accelerated by the wet and hot subtropical climate (García et al. 2001). The positive effect of temperature on the chemical weathering rates of silicate minerals is described by Gaillardet et al. (1999), Millot et al. (1999) and White et al. (1999), and noted by Herczeg (2001) in terms of the high rates of soil CO_2 and organic acid production in warm climates such as the Atherton Tablelands. High concentrations of SiO_2 in the Atherton groundwaters (average of 93 mg/L) indicate the presence of volcanic glass. Benedetti et al. (1999) and Gérard et al. (1999), for example, found that the weathering of glass is characterized by the release of Ca^{2+} and Mg^{2+}, as well as Si^{4+}, Na^+, and K^+ and is the major control on the compositions of stream and spring waters around the volcano Mount Cameroon in central Africa. The effect of basaltic glass on solution composition is supported by Oelkers et al. (1999).

The average Al^{3+}/SiO_2 ratio (in mmol/L) in the Atherton groundwaters is 1.5×10^{-3}, with a maximum value of 4.2×10^{-2}. Thus, aluminum appears to be relatively immobile in this system; it is therefore assumed that aluminum is conserved in the solid phases and stability diagrams for some of the common silicate minerals can be constructed. Mineral stability diagrams for the calcium, magnesium, and sodium aluminosilicate systems for the Atherton basalt groundwaters (Locsey and Cox 2002b) indicate that the groundwaters are at equilibrium with respect to kaolinite and/or smectite clays.

The saturation index can also be useful for examining potential secondary phases and the dissolution of primary minerals in an aquifer system. Saturation index calculations for aluminosilicates are limited, however, by low Al^{3+} concentrations and the assumption of idealized, end-member mineralogies (Fryar et al. 2001).

The saturation states of the Atherton basalt groundwaters with respect to some of the primary minerals present in the Atherton basalts, that is, the plagioclase feldspars (albite and anorthite) and K-feldspar are shown in Fig. 7 as a function of pH. The groundwaters are mostly at equilibrium or saturated with respect to K-felspar and approach equilibrium with respect to the plagioclase feldspars with increasing pH.

The Atherton basalt groundwaters are at equilibrium or saturated with respect to the major secondary minerals, kaolinite, smectite (Ca-montmorillonite), and gibbsite (Fig. 8). The groundwaters also tend to be saturated with respect to goethite and hematite, with average saturation indices for these minerals of 3.0 and 4.1, respectively. These oxidation products are common accessory minerals in the basalt sequence, as discussed above.

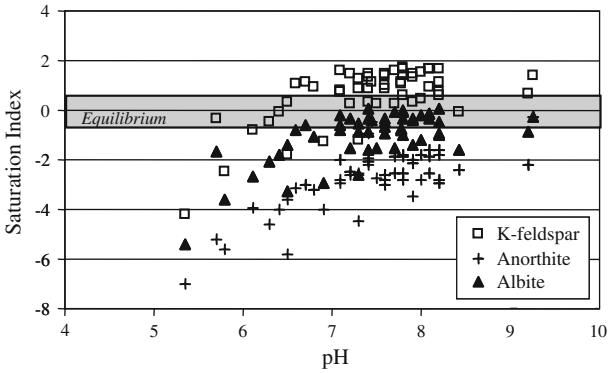

Fig. 7 Groundwater saturation indices with respect to albite, anorthite, and K-feldspar as a function of pH

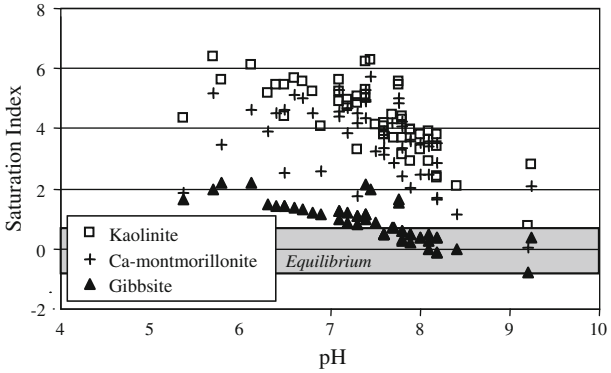

Fig. 8 Groundwater saturation indices with respect to kaolinite, Ca-montmorillonite, and gibbsite as a function of pH

Although the Atherton basalt groundwater plot to the right of the quartz line on the silicate stability diagrams and the saturation indices indicate that the groundwaters are saturated with respect to quartz (Locsey and Cox 2002b), some authors consider quartz to be kinetically unreactive at low temperatures and note that it rarely precipitates or dissolves at a significant rate; amorphous silica, however, precipitates and dissolves relatively rapidly (Drever 1997). More recent studies (Rimstidt 1997; Gunnarsson and Arnórsson 1999) have shown, however, that quartz is more soluble at low temperatures than has generally been accepted. Fridriksson et al. (1999) note that celadonite typically forms before silica in Tertiary basalts in eastern Iceland and minerals such as opal, chalcedony, and quartz also precipitate in vesicles and along fractures. Precipitation of microcrystalline silica has also been observed, for example, in the basalts of the eastern Snake River Plain, Idaho (Wood and Low 1986) and Craig and Loughnan (1964) observed that secondary silica occurs as chalcedonic quartz rimmed with opal in weathered basalt profiles in eastern New South Wales. The composition of the Atherton basalt groundwaters and the identification of small percentages of quartz by XRD throughout much of the basalt sequence indicate that quartz and/or other phases of crystalline or amorphous silica precipitate in these basalts.

The Atherton basalt groundwaters are also at equilibrium or saturated with respect to calcite and dolomite at pH values >7.5 (Locsey and Cox 2002b). The only carbonate mineral identified in the Atherton basalt samples using XRD is siderite. However,

carbonate infilling of vesicles has commonly been observed in the Atherton basalts (Buck 1999), and minerals such as calcite and dolomite are known to precipitate in basalt (e.g., Craig and Loughnan 1964; Carr et al. 1980; Deutsch et al. 1982; Wood and Low 1986; Gíslason et al. 1993; Pawar 1993). Pawar (1993) proposes that recharge waters enriched in CO_2 may encounter lower partial pressures of CO_2 upon downward penetration toward the deeper unsaturated/saturated zone, resulting in the loss (by degassing) of CO_2. Where the partial pressure of CO_2 becomes insufficient for the soluble calcium bicarbonate to remain stable, calcium carbonate may precipitate (Craig and Loughnan 1964); provided that the concentrations of Ca^{2+} and HCO_3^- are sufficiently high, the removal of CO_2 may lead to the precipitation of calcite (Pawar 1993) as shown in Equation 1.

$$Ca^{2+} + HCO_3^- \rightarrow CaCO_3 + H^+ \quad (1)$$

The likelihood of dolomite forming from aqueous solution is related to the salinity of the groundwater and the ratio of Mg^{2+} to Ca^{2+} ions in solution (Folk and Land 1975). The work of Folk and Land (1975) indicates that dolomite can form from fresh waters with TDS <350 ppm provided that the Mg^{2+}/Ca^{2+} ratios are greater than approximately 1:1; for waters of higher salinity, higher Mg^{2+}/Ca^{2+} ratios are required. As the Atherton groundwaters are of low salinity (TDS generally <250 ppm) and approximately 79% of the basalt groundwater samples have Mg^{2+}/Ca^{2+} ratios of 1–2: 1 and a further 6% of samples have ratios of more than 2:1, dolomite formation, as shown in Eq. 2, is possible.

$$Mg^{2+} + Ca^{2+} + 2HCO_3^- \rightarrow CaMg(CO_3)_2 + 2H^+. \quad (2)$$

The reactions shown in Eqs. 1 and 2 release protons to solution and thus provide a pH buffer. A small percentage of the groundwaters sampled also have concentrations of Fe^{2+} more than 5% that of Ca^{2+} (including groundwaters from bore 11000128), and some of the groundwaters are approaching equilibrium with respect to siderite, indicating that siderite is stable relative to calcite in parts of this aquifer system (Berner 1971). This is supported by the mineralogical analyses presented above, showing that siderite is a common accessory mineral throughout much of the basalt sequence.

In studies of basaltic groundwaters in Iceland, Arnórsson et al. (1983) and Arnórsson (1999) found that most of the aqueous components (except Cl^- and sometimes SO_4^{2-}) are controlled by equilibria with secondary minerals when temperatures are <40°C and sometimes as low as 10–20°C. Wood and Low (1986) similarly found that the basaltic groundwaters of the eastern Snake River Plain, Idaho, are supersaturated with the secondary clay mineral calcium-smectite, in a cold climate where the average annual temperature is approximately 8°C. It seems that thermal conditions are not necessarily required for the relatively fast reaction of basaltic minerals and equilibration with secondary clays. Arnórsson (1999) attributed the close approach to mineral–solution equilibria in the low-temperature Icelandic basalt groundwaters to the high reactivity of the mafic minerals in basalt, the low content of soluble salts, and the generally limited supply of CO_2 to water from decaying organic soil due to sparse vegetation cover. If acids are supplied to the water in relatively large quantities, however, more reaction with the rock forming minerals is required to bring the system to equilibrium than would be the case when the acid supply is limited (Arnórsson 1999).

As some parts of the Atherton Tablelands have dense vegetation and exposed rock is rare in comparison to the terrain of many parts of Iceland for example, supply of organic CO_2 to groundwaters in the study area may be substantially higher. Calculations based on the pH and alkalinity measurements using the computer program PHREEQC give values of

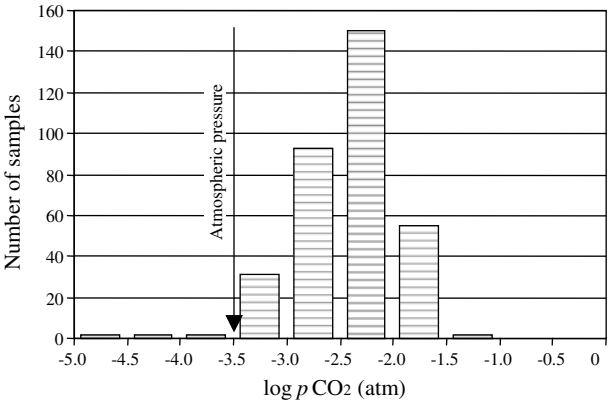

Fig. 9 Distribution of equilibrium partial pressure of CO_2 (on a log scale)

equilibrium partial pressure of CO_2 (pCO_2) from $10^{-1.4}$ to $10^{-4.7}$ atm. The distribution of the computed pCO_2 values (on a log scale) is shown in Fig. 9. Compared to the present value of pCO_2 in the atmosphere of $10^{-3.5}$ atm (Appelo and Postma 1996), the groundwater data indicate that rainwater charged with CO_2 has acquired additional CO_2 by the decomposition of organic matter and plant root respiration in the soils. Values for groundwater pCO_2 that range from 5 to 100 times greater than those for atmospheric values seem reasonable for tropical environments (Stallard and Edmond 1987). In a groundwater study in the Northern Territory in an area with a monsoonal tropical climate, Herczeg and Payne (1992) similarly found groundwater pCO_2 values range from 10 to more than 100 times atmospheric pCO_2.

The high initial pCO_2 values of the Atherton groundwaters are progressively lowered by CO_2 consumption during water–rock interaction. Groundwaters strongly depleted in CO_2 (values $<10^{-3.5}$ atm) are those that are approaching or are at equilibrium with the primary aluminosilicate minerals. As the Atherton Tablelands basalt groundwaters are mostly in equilibrium with the major secondary minerals (Fig. 8), sufficient mineral reactions must be occurring to equilibrate these groundwaters with the secondary mineral phases, despite the high CO_2 contributions. The high annual temperatures in the study area may be an important factor influencing the reaction rates.

9.2 Summary of Hydrogeochemical Processes

A model for the evolution of the Atherton basalt groundwaters can be described by the following processes—recharge to the aquifer of CO_2-charged rain water, where the water reacts with the aquifer minerals, utilizing the H_2CO_3 derived from organic matter in the soil zone. Such interaction between water and rock forming minerals is described by Garrels and Mackenzie (1967), Helgeson et al. (1969), and Arnórsson (1999) as a titration process where the minerals may be regarded as bases reacting with an acid (i.e., H_2CO_3) dissolved in the water, producing secondary minerals and dissolved salts. The silicate minerals undergoing weathering reactions are predominantly pyroxene and plagioclase feldspars, and kaolinite is the dominant clay mineral forming (Table 5). Water–rock interaction in the saturated zone is likely to be a closed system process (with high initial pCO_2), whereby the silicate weathering reactions consume CO_2, and cations, HCO_3^- and H_4SiO_4, are released to solution, and the pH increases.

Table 5 Generalized mass balance for the Atherton Tablelands basalt groundwaters (units are μmol/L)

	Na^+ (μmol/L)	Ca^{2+} (μmol/L)	Mg^{2+} (μmol/L)	K^+ (μmol/L)	HCO_3^- (μmol/L)	SO_4^{2-} (μmol/L)	Cl^- (μmol/L)	H_4SiO_4 (μmol/L)
Average basalt groundwater composition	390	290	410	50	1430	14	321	980
Correction for atmospheric input	160	220	370	0	1410	0	0	980
Dissociation of olivine								
$100Mg_2SiO_4 + 400CO_2 + 400H_2O = 200Mg^{2+} + 100H_4SiO_4 + 400HCO_3^-$								
Remainder	160	220	170	0	1010	0	0	880
Weathering of augite to kaolinite								
$240[CaMg_{0.7}Al_{0.6}Si_{1.7}]O_6 + 816CO_2 + 1080H_2O = 72Al_2Si_2O_5(OH)_4 + 240Ca^{2+} + 168\ Mg^{2+} + 264H_4SiO_4 + 816HCO_3^-$								
Remainder	160	−20	2	0	194	0	0	616
Weathering of albite to kaolinite								
$230NaAlSi_3O_8 + 230CO_2 + 1265H_2O = 115Al_2Si_2O_5(OH)_4 + 230Na^+ + 460H_4SiO_4 + 230HCO_3^-$								
Remainder	−70	−20	2	0	−36	0	0	156
Precipitation of calcite								
$20Ca^{2+} + 20HCO_3^- = 20CaCO_3 + 20H^+$								
Remainder[a]	−70	0	2	0	−16	0	0	156
Overall reaction								
100 Olivine + 240 Augite + 230 Albite ($+H_2O + CO_2$) = 187 Kaolinite + 20 Calcite + 230 Na^+ + 220 Ca^{2+} + 368 Mg^{2+} + 824 H_4SiO_4 + 1426 HCO_3^-								

[a] Values for Mg^{2+} and HCO_3^- are effectively zero; 84% of the H_4SiO_4 is accounted for and excess Na^+ is generated

High concentrations of silica in the groundwaters lead to saturation with respect to silica and precipitation of amorphous or crystalline phases. Weathering products such as hematite, goethite, gibbsite, siderite, pyrite, and zeolites also form. When the concentration of Ca^{2+} is sufficiently high (in addition to elevated pH), calcite saturation occurs, leading to its precipitation in the vesicles and along the fracture planes of the basalt. If the concentrations of Mg^{2+} are also sufficiently high, the groundwaters may become saturated with respect to dolomite and precipitation may occur under suitable conditions.

10 Hydrogeochemical Mass Balance

Based on an average basaltic groundwater composition for the study area, the likely reactions that give rise to the composition were deduced using a mass balance approach. The aqueous geochemical modeling code PHREEQC (Parkhurst and Appelo 1999) was used to solve the inverse problem with the inputs being an initial water composition, a final water composition, and a list of phases that may dissolve or precipitate. The output is a list of possible reactions involving the listed minerals that satisfy the mass balance constraints (Drever 1997). A disadvantage with this type of modeling, as discussed by Keller et al. (1991) and Drever (1997), is that solutions, particularly of silicate weathering reaction schemes, are rarely unique; several different combinations of minerals may satisfy the constraints.

Obtaining a mass balance for an aquifer system that is unconfined, with relatively dilute groundwaters and where compositional changes along flow paths are small, is difficult (Fryar et al. 2001). In a method similar to that used by Garrels and Mackenzie (1967) and Wood and Low (1986), a generalized mass balance for the Atherton basalt groundwaters was calculated and is presented as a series of reactions for the major weathering and precipitating minerals (Table 5). Dissociation of olivine releases Mg^{2+}, H_4SiO_4, and HCO_3^- to solution, the weathering of augite to kaolinite releases Mg^{2+}, Ca^{2+}, H_4SiO_4, and HCO_3^-, and the weathering of the plagioclase feldspar albite releases Na^+, H_4SiO_4, and HCO_3^-. Calcite is precipitated, consuming a small amount of Ca^{2+} and HCO_3^- ions. The simplified mass balance presented here does not take into account several of the minor primary and secondary mineral phases or volcanic glass present in the basalt.

It is noted that as an average groundwater composition has been used in the mass balance, the charge is unbalanced, which may in part account for the excess of excess of Na^+ ions released to solution for the set of weathering reactions presented in Table 5. A more probable chemical weathering model for the Atherton Tablelands basalt groundwaters is one in which the plagioclase feldspar content comprises intermediate phases in the albite to anorthite solid solution series, rather than the idealized end-members presented here. The set of weathering reactions in Table 5 also account for only 84% of the H_4SiO_4 released to solution; the weathering of volcanic glass would provide additional H_4SiO_4. The generalized mass balance presented in Table 5 demonstrates, however, that a combination of aluminosilicate mineral weathering reactions is the primary control on the composition of these basalt groundwaters.

11 Conclusions

The sequence of basaltic rocks in the Atherton Tablelands region shows considerable variation in mineralogical content and degree of weathering. The primary minerals in the

basalts are predominantly pyroxenes and feldspars, with minor olivine and other accessory minerals, as well as amorphous material, which is probably volcanic glass or organic matter. Secondary minerals present in the basalt are predominantly kaolinite, and smectites, with iron and aluminum weathering products, carbonates, and zeolites also present.

Groundwater in the Atherton basalts may occur in both vesicular and fractured rock. While the work presented here indicates that the groundwater is more likely to be stored within fresh or weathered vesicular layers, fractures are considered important pathways for groundwater movement in this aquifer system.

The weathering of aluminosilicate minerals is interpreted to be the major control on the composition of the Atherton basalt groundwaters. A general weathering model can be derived for the chemical weathering of these basalt rocks: precipitation + CO_2 (atmospheric + soil) + pyroxene + feldspars + olivine yields H_4SiO_4, HCO_3^-, Mg^{2+}, Na^+, Ca^{2+} + kaolinite and smectite clays + amorphous or crystalline silica + accessory minerals (hematite, goethite, gibbsite, carbonates, zeolites, and pyrite).

While the plagioclase feldspars are the primary source of Na^+ for these basalt groundwaters, the enrichment of Na^+ (and to a lesser extent Mg^{2+}) relative to Ca^{2+} may be due to either ion-exchange reactions (releasing Na^+ to solution) or the precipitation of carbonate minerals, which act as sinks for Ca^{2+} and Mg^{2+}.

References

Alberti A, Vezzalini G, Galli E, Quartieri S (1996) The crystal structure of gottardiite, a new zeolite. Eur J Mineral 8:69–75

Appelo CAJ, Postma D (1996) Geochemistry, groundwater and pollution. Balkema, Rotterdam, p 536

Arnórsson S (1999) Invited lecture: progressive water–rock interaction and mineral-solution equilibria in groundwater systems. In: Ármannsson H (ed) Geochemistry of the earth's surface. Balkema, Rotterdam, pp 471–474

Arnórsson S, Gunnlaugsson E, Svavarsson H (1983) The chemistry of geothermal waters in Iceland: II. Mineral equilibria and independent variables controlling water compositions. Geochim Cosmochim Acta 47:547–566

Barshad I (1966) The effect of a variation in precipitation on the nature of clay mineral formation in soils from acid and basic igneous rocks. In: Heller L, Weiss A (eds) Proceedings of the international clay conference, vol 1. Israel Program for Scientific Translations, Jerusalem, pp 167–173

Bean JA (1999) A conceptual model of groundwater behaviour in the Atherton Basalt Province, Atherton Tablelands, Far North Queensland. Unpublished MAppSc thesis, Queensland University of Technology, Brisbane, p 159

Benedetti MF, Menard O, Noack Y, Carvalho A, Nahon D (1994) Water–rock interactions in tropical catchments: field rates of weathering and biomass impact. Chem Geol 118:203–220

Benedetti MF, Boulegue J, Dia A, Bulourde M, Chauvel C, Chabaux F, Riotte J, Fritz B, Gérard M, Bertaux J, Etame J, Deruelle B, Ildefonse PH (1999) The weathering of mount cameroon: 2. Water geochemistry. In: Ármannsson H (ed) Geochemistry of the earth's surface. Balkema, Rotterdam, pp 365–367

Berner RA (1971) Principles of chemical sedimentology. McGraw-Hill, New York, p 240

Bish DL, Post JE (1989) Sample preparation for x-ray diffraction. Rev Mineral 20:72–99. Mineralogical Society of America, Washington, DC

Bluth GJS, Kump LR (1994) Lithologic and climatologic controls of river chemistry. Geochim Cosmochim Acta 58:2341–2359

Buck LJ (1999) Physical features of volcanism and their relationship to groundwater, Atherton Basalt Province, North Queensland. Unpublished BAppSc(Hons) thesis, Queensland University of Technology, Brisbane p 178

Carr RG, Rodgers KA, Black PM (1980) The chemical and mineralogical changes accompanying the laterization of basalt at Kerikeri, North Auckland. J R Soc N Z 10(3):247–258

Chalmers RO (1967) Australian rocks, minerals and gemstones. Angus and Robertson, Sydney, p 398

Cleaves ET, Fisher DW, Bricker OP (1974) Chemical weathering of serpentinite in the Eastern Piedmont of Maryland. Geol Soc Am Bull 85:437–444
Cook PG, Herczeg AL, Mcewan KL (2001) Groundwater recharge and stream baseflow, Atherton Tablelands, Queensland. CSIRO Land and Water Technical Report 08/01, p 84
Craig DC, Loughnan FC (1964) Chemical and mineralogical transformation accompanying the weathering of basic volcanic rocks from New South Wales: Australia. Aust J Soil Res 2:218–234
Crovisier JL, Honnorez J, Fritz B, Petit JC (1992) Dissolution of subglacial volcanic glasses from Iceland: laboratory study and modelling. Appl Geochem Suppl Issue 1:55–81
Deer WA, Howie RA, Zussman J (1966) An introduction to the rock forming minerals. Longman Group, London, p 528
Deutsch WJ (1997) Groundwater geochemistry–fundamentals and applications to contamination. Lewis Publishers, Boca Raton, p 221
Deutsch WA, Jenne EA, Krupka KM (1982) Solubility equilibria in basalt aquifers: the Columbia Plateau, eastern Washington, USA. Chem Geol 36:15–34
Drever JI (1997) The geochemistry of natural waters, surface and groundwater environments. Prentice Hall, Upper Saddle River, p 436
Ecker A (1976) Groundwater behaviour in Tenerife, volcanic island (Canary Islands, Spain). J Hydrol 28: 73–86
Edmunds WM, Carrillo-Rivera JJ, Cardona A (2002) Geochemical evolution of groundwater beneath Mexico City. J Hydrol 258:1–24
Eggleton RA, Foudoulis C, Varkevisser D (1987) Weathering of basalt: changes in rock chemistry and mineralogy. Clays Clay Min 35(3):161–169
Faure G (1998) Principles and applications of geochemistry. Prentice Hall, Upper Saddle River, p 600
Folk RL, Land LS (1975) Mg/Ca ratio and salinity: two controls over crystallization of dolomite. Am Assoc Petrol Geol Bull 59(1):60–68
Fridriksson TH, Neuhoff PS, Bird DK, Arnórsson S (1999) Clays and zeolites record alteration history at Teigarhorn, eastern Iceland. In: Ármannsson H (ed) Geochemistry of the earth's surface. Balkema, Rotterdam, pp 377–380
Fryar AE, Mullican WF III, Macko SA (2001) Groundwater recharge and chemical evolution in the southern High Plains of Texas, USA. Hydrogeol J 9(6):522–542
Gaillardet J, Allègre CJ, Dupré B (1999) Invited lecture: Intensities and fluxes of global silicate weathering deduced from large river study. In: Ármannsson H (ed) Geochemistry of the earth's surface. Balkema, Rotterdam, pp 75–77
Galli E, Quartieri S, Vezzalini G, Alberti A (1995) Boggsite and tschernichite-type zeolites from Mt. Adamson, Northern Victoria Land (Antarctica). Eur J Mineral 7:1029–1032
Galli E, Quartieri S, Vezzalini G, Alberti A (1996) Gottardiite, a new high-silica zeolite from Antarctica: the natural counterpart of synthetic NU-87. Eur J Mineral 8:687–693
García MG, Hidalgo M del V, Blesa MA (2001) Geochemistry of groundwater in the alluvial plain of Tucumán province, Argentina. Hydrogeol J 9(6):597–610
Garrels RM (1967) Genesis of some ground waters from igneous rocks. In: Abelson PH (ed) Researches in Geochemistry 2. Wiley, New York, pp 405–420
Garrels RM, Mackenzie FT (1967) Origin of the chemical compositions of some springs and lakes. In: Stumm W (ed) Equilibrium concepts in natural water systems: a symposium, advances in Chemistry series 67. American Chemical Society, Washington, pp 222–242
Gérard M, Bertaux J, Ildefonse PH, Bulourde M, Chauvel C, Dia A, Benedetti M, Boulègue J, Chabaux F, Fritz B, Etame J, Ngounouno I, Deruelle B (1999) Weathering of mount Cameroon: 1. Mineralogy and geochemistry. In: Ármannsson H (ed) Geochemistry of the earth's surface. Balkema, Rotterdam, pp 381–384
Gibbs RJ (1970) Mechanisms controlling world water chemistry. Science 170:1088–1090
Gíslason SR, Arnórsson S (1993) Dissolution of primary basaltic minerals in natural waters: saturation state and kinetics. Chem Geol 105:117–135
Gíslason SR, Veblen DR, Livi KJT (1993) Experimental meteoric water–basalt interactions: characterization and interpretation of alteration products. Geochim Cosmochim Acta 57:1459–1471
Gíslason SR, Arnórsson S, Ármannsson H (1996) Chemical weathering of basalt in southwest Iceland: effects of runoff, age of rocks and vegetative/glacial cover. Am J Sci 296:837–907
Gunnarsson I, Arnórsson S (1999) New data on the standard Gibbs energy of H_4SiO_4 and its effect on silicate solubility. In: Ármannsson H (ed) Geochemistry of the earth's surface. A. A. Balkema, Rotterdam, pp 449–452
Hamilton WR, Woolley AR, Bishop AC (1989) Minerals, rocks and fossils. Hamlyn, London, p 320
Head B (1979) Zeolites of the Garrawilla volcanics, New South Wales. Aust Mineral 23:109–111

Helgeson HC, Garrels RM, Mackenzie FT (1969) Evaluation of irreversible reactions in geochemical processes involving minerals and aqueous solutions II. Applications. Geochim Cosmochim Acta 33: 455–481

Herczeg AL (2001) Can major ion chemistry be used to estimate groundwater residence time in basaltic aquifers? In: Cidu R (ed) Water–rock interaction WRI-10. A. A. Balkema, Lisse, pp 529–532

Herczeg AL, Payne TE (1992) Recharge and weathering processes in fractured rock aquifers in Northern Australia. In: Kharaka YK, Maest AS (eds) Water–rock interaction WRI-7. Balkema, Rotterdam, pp 561–564

Hill IG, Worden RH, Meighan IG (2000) Geochemical evolution of a palaeolaterite: the Interbasaltic formation, Northern Ireland. Chem Geol 166:65–84

Hounslow AW (1995) Water quality data–analysis and interpretation. Lewis Publishers, Boca Raton, p 397

Howard DG, Tschernich RW, Smith JV, Klein GL (1990) Boggsite, a new high silica zeolite from Goble, Columbia County, Oregon. Am Mineral 75:1200–1204

Keller CK, van der Kamp G, Cherry JA (1991) Hydrogeochemistry of a clayey till 1. Spatial variability. Water Resour Res 27(10):2543–2554

Leach LM (1986) Groundwater resources of the Atherton basalt, Atherton Shire. Queensland Water Resources Commission, Mareeba

Liou JG (1971) Analcime equilibria. Lithos 4:389–402

Locsey KL, Cox ME (2000) Chemical character of groundwater in a basalt aquifer, North Queensland, Australia. In: Sililo O et al. (eds) Groundwater: past achievements and future challenges. Proceedings of the XXXth international congress of the international association of hydrogeologists, Cape Town, Balkema, Rotterdam, pp 555–560

Locsey KL, Cox ME (2002a) Statistical and hydrochemical methods to compare basalt- and basement rock-hosted groundwaters: Atherton Tablelands, north-eastern Australia. Environ Geol. doi:10.1007/s00254-002-0667-z

Locsey KL, Cox ME (2002b) Hydrochemical variability as a tool for defining groundwater movement in a basalt aquifer: the Atherton Tablelands, North Queensland. In: Proceedings of the international association of hydrogeologists international groundwater conference: balancing the groundwater budget, Darwin, 12–17 May 2002

Lyle P (1974) A petrological and petrochemical study of Tertiary basaltic rocks in north-east Ireland and north-west Ireland. Unpublished PhD thesis, Queen's University, Belfast

Middelburg JJ, van der Weijden CH, Woittiez JRW (1988) Chemical processes affecting the mobility of major, minor and trace elements during the weathering of granitic rocks. Chem Geol 68:253–273

Millot R, Gaillardet J, Allègre CJ, Dupré B (1999) Silicate weathering rates in the Mackenzie river basin, North-West Territories, Canada. In: Ármannsson H (ed) Geochemistry of the earth's surface. Balkema, Rotterdam, pp 115–118

Nesbitt HW, Wilson RE (1992) Recent chemical weathering of basalts. Am J Sci 292:740–777

Nordstrom DK, Munoz JL (1994) Geochemical thermodynamics. Blackwell Scientific Publications, Boston, p 493

Oelkers EH, Schott J, Gíslason SR (1999) Invited lecture: A general mechanism for multi-oxide solid dissolution and its application to basaltic glass. In: Ármannsson H (ed) Geochemistry of the earth's surface. Balkema, Rotterdam, pp 413–416

Parkhurst DL, Appelo CAJ (1999) User's guide to PHREEQC (version 2)—a computer program for speciation, batch-reaction, one-dimensional transport, and inverse geochemical calculations. United States Geological Survey Water-Resources Investigations Report 99–4259, p 312

Pawar NJ (1993) Geochemistry of carbonate precipitation from the ground waters in basaltic aquifers: an equilibrium thermodynamic approach. J Geol Soc India 41:119–131

Pawar NJ, Pawar JB, Kumar S, Supekar A (2008) Geochemical eccentricity of ground water allied to weathering of basalts from the Deccan Volcanic Province, India: Insinuation on CO_2 consumption. Aquat Geochem 14:41–71

Pearce BR (2002) Report on compilation of a geological conceptual model for the Atherton Tableland Basalts. Queensland Department of Natural Resources and Mines, Brisbane

Pearce BR, Durick AM (2002) Assessment and management of basalt aquifers on the Atherton Tablelands, North Queensland, Australia. In: Proceedings of the international association of hydrogeologists international groundwater conference: balancing the groundwater budget, Darwin, 12–17 May 2002

Phillipo S, Naud J, Verkaeren J (1997) Geochemical evaluation of the Lueshe niobium deposit by Reitveld quantitative X-ray diffraction. Appl Geochem 12:175–180

Plummer LN (1992) Geochemical modeling of water–rock interaction: past, present, future. In: Kharaka YK, Maest AS (eds) Water–rock interaction WRI-7. Balkema, Rotterdam, pp 23–33

Plummer LN, Back W (1980) The mass balance approach: application to interpreting the chemical evolution of hydrologic systems. Am J Sci 280:130–142
Price RC, Gray CM, Frey FA (1997) Strontium isotopic and trace element heterogeneity in the plains basalts of the Newer Volcanic Province, Victoria, Australia. Geochim Cosmochim Acta 61:171–192
Prudêncio MI, Sequeira Braga MA, Paquet H, Waerenborgh JC, Pereira LCJ, Gouveia MA (2002) Clay mineral assemblages in weathered basalt profiles from central and southern Portugal: climatic significance. Catena 49:77–89
Reitveld HM (1969) A profile refinement method for nuclear and magnetic structures. J Appl Crystallogr 2:65–71
Rimstidt JD (1997) Quartz solubility at low temperatures. Geochim Cosmochim Acta 44:1683–1699
Sheldrick MKM (1999) Stratigraphic interpretation of a lava field using petrogenetic modelling. Unpublished BAppSc(Hons) thesis, Queensland University of Technology, Brisbane, p 57
Stallard RF, Edmond JM (1987) Geochemistry of the Amazon 3. Weathering chemistry and limits to dissolved inputs. J Geophys Res 92(C8):8293–8302
Stephenson PJ (1989) Northern Queensland. In: Johnson RW (ed) Intraplate volcanism in Eastern Australia and New Zealand. Cambridge University Press, Cambridge, pp 89–97
Stephenson PJ, Griffin TJ, Sutherland FL (1980) Cainozoic volcanism in northeastern Australia. In: Henderson RA, Stephenson PJ (eds) The Geology and Geophysics of Northeastern Australia. Geological Society of Australia, Queensland Division, Brisbane, pp 349–374
Sutherland FL (1983) Timing, trace and origin of basaltic migration in eastern Australia. Nature 305(8): 123–126
Tschernich RW (1992) Zeolites of the world. Geoscience Pres Inc, Phoenix, p 563
Walker GPL (1960) The amygdale minerals in the Tertiary lavas of Ireland: III. regional distribution. Mineral Mag 32:503–527
Wellman P, McDougall I (1974) Cainozoic igneous activity in eastern Australia. Tectonophysics 23:49–65
White AF, Claassen HC, Benson LV (1980) The effect of dissolution of volcanic glass on the water chemistry in a tuffaceous aquifer, Rainier Mesa, Nevada. United States Geological Survey Water-Supply Paper 1535-Q. United States Government Printing Office, Washington, DC, p 34
White AF, Bullen TD, Vivit DV, Schulz MS, Blum AE (1999) Invited lecture: the effect of climate on chemical weathering of silicate rocks. In: Ármannsson H (ed) Geochemistry of the earth's surface. Balkema, Rotterdam, pp 79–82
Wood WW, Low WH (1986) Aqueous geochemistry and diagenesis in the eastern Snake River plain aquifer system, Idaho. Geol Soc Am Bull 97:1456–1466